

Antiferromagnetic domain walls under spin-orbit torque

G. Theodorou^{1,2} and S. Komineas^{1,2}

¹*Department of Mathematics and Applied Mathematics,
University of Crete, 70013 Heraklion, Crete, Greece*

²*Institute of Applied and Computational Mathematics, FORTH, Heraklion, Crete, Greece*

(Dated: September 29, 2025)

Domain walls in antiferromagnets under a spin-polarized current present rich dynamics that is not observed in ferromagnets, and it is tunable by the current polarization. Precessional dynamics is obtained for perpendicular spin polarization, in agreement with expectations in older works. Propagating walls are obtained for an in-plane polarization. We obtain the velocity as a function of current by a perturbation method for low velocities, and the wall profile is found to lack a definite parity. For high velocities, the main features of the wall profile are obtained by a direct solution of an equation that is valid in a limiting case. We discuss the magnetization of the dynamical walls and find that this can become large, providing a potential method for observations. Oscillatory motion of domain walls is obtained for spin polarization that has both perpendicular and in-plane components, and an analytical description is given.

I. INTRODUCTION

Antiferromagnetic domain walls have attracted attention since decades ago [1, 2] and their study has led to remarkable conclusions [3]. Interest has grown in recent years as antiferromagnetic order can now be observed in a more efficient way and domain walls can be directly imaged [4–7]. In addition, experimental techniques allow for optical [8] and electrical [7, 9] manipulation of domain walls, while current-induced switching can be achieved by domain wall motion [10]. The efficient manipulation of antiferromagnets (AFMs) has the potential to lead to significant advantages over the widely used ferromagnets, as antiferromagnetic order produces no stray fields, thus making it easier to control and also robust under moderate external fields.

The dynamics in antiferromagnets is described by extensions of the nonlinear σ -model for the Néel vector [1, 2] and is radically different from the dynamics of magnetization in ferromagnets, potentially leading to advantages. It allows for a wider range of dynamical behaviors including Newtonian and relativistic dynamics [11–14] as the σ -model is second order in time. Dynamics in AFM can be probed by spin-polarized currents, and antiferromagnetic spintronics is now being developed in a fashion analogous to ferromagnets [15, 16]. Spin-orbit torques drive antiferromagnetic domain walls faster than ferromagnetic domain walls [17–19] while they can also be manipulated by spin-transfer torques [20–22].

We study the dynamics of antiferromagnetic domain walls under spin-orbit torque. We find that precessional dynamics, analogous to that discussed in the conservative model [3, 12, 23], is spontaneously obtained as a steady state. Propagation of a domain wall with a constant velocity is also obtained, but this is not the result of a simple Lorentz transformation of the static wall. For a spin current polarization that has both an in-plane and a perpendicular component, oscillations of the domain wall are obtained where the wall moves between two positions in a periodic motion. The present study is based on a model that describes antiferromagnetic dynamics under spin-torque, and it is going beyond the idealized σ -model regarding the methods used and the results obtained. Our findings fully take into account the breaking of Lorentz invariance of the model due to the damping term.

We discuss the magnetic moment carried by the studied antiferromagnetic textures. This is of particular importance, as it could allow for the observation of textures and give a handle to make them functional. For domain walls, a net magnetic moment has been theoretically predicted within a strictly one-dimensional model [11, 24], and it has subsequently been observed [25, 26]. For a dynamical wall, the time dependence of the Néel order parameter gives rise to an additional magnetic moment.

The paper is organized as follows. Sec. II introduces the discrete and continuum models. Sec. III is a study of the precessional dynamics of domain walls. Sec. IV is a study of propagating domain walls. Sec. V introduces oscillatory motion of domain walls. Sec. VI contains our concluding remarks.

II. THE MODEL

We consider a spin chain \mathbf{S}_i with antiferromagnetic exchange, Dzyaloshinskii-Moriya (DM) interaction, and perpendicular anisotropy. The magnetic energy is

$$E^d = \sum_i J \mathbf{S}_i \cdot \mathbf{S}_{i+1} + D \hat{\mathbf{e}}_2 \cdot (\mathbf{S}_i \times \mathbf{S}_{i+1}) + \frac{K}{2} [s^2 - (\mathbf{S}_i)_3^2], \quad (1)$$

where J, D, K are positive parameters, and the spin variables have length $|\mathbf{S}_i| = s$ with s a dimensionless number. The energy E^d has units of inverse time. We will mainly study the case with no DM interaction ($D = 0$), but we will comment on the effect of the DM in most of the cases studied. We will study antiferromagnetic domain walls and their dynamics. For probing the dynamics of the antiferromagnet, we will assume spin torque produced by polarized electrons injected into the sample. The equations of motion for the spins are

$$\frac{\partial \mathbf{S}_i}{\partial t} = \mathbf{S}_i \times \left(\mathbf{F}_i + \tilde{\alpha} \frac{\partial \mathbf{S}_i}{\partial t} - \tilde{\beta} \mathbf{S}_i \times \hat{\mathbf{p}} \right), \quad \mathbf{F}_i = -\frac{\partial E^d}{\partial \mathbf{S}_i} \quad (2)$$

where $\tilde{\alpha}$ is the damping parameter, $\hat{\mathbf{p}}$ is the spin current polarization and

$$\tilde{\beta} = \frac{J_e A b}{e s^2}$$

is the spin torque parameter, with J_e the current density, A the area occupied by a single spin, e the electron charge, and b a constant that is related to the degree of spin polarization.

For a theoretical study, a continuum approximation of the equations of motion is necessary. A continuum model is usually obtained when we consider a dimerization of the spin lattice and define the Néel vector \mathbf{n}_α and magnetization \mathbf{m}_α that are the normalized difference and sum of neighboring spins, respectively, at each dimer site α . While we study configurations that vary in one dimension, we assume that the actual spin lattice is two-dimensional, such as a film (this requires to consider spins $\mathbf{S}_{i,j}$ and generalize the energy (1) accordingly). Instead of dimers, we consider tetramers since they comply with the symmetry of a two-dimensional square spin lattice [27]. The distance between neighboring tetramer sites is defined to be 2ϵ where

$$\epsilon = \sqrt{\frac{K}{J}}$$

is a small parameter. In the limit $\epsilon \rightarrow 0$, a continuous Néel vector field $\mathbf{n} = \mathbf{n}(x, \tau)$ is obtained, with $|\mathbf{n}| = 1$, where x and τ are scaled space and time variables. The equation of motion in the continuum is an extension of the nonlinear σ -model for the Néel vector \mathbf{n} with the addition of damping and a spin torque term [2, 28, 29],

$$\mathbf{n} \times (\ddot{\mathbf{n}} - \mathbf{f} - \beta \mathbf{n} \times \hat{\mathbf{p}} + \alpha \dot{\mathbf{n}}) = 0, \quad \mathbf{f} = \mathbf{n}'' - 2\lambda \hat{\mathbf{e}}_2 \times \mathbf{n}' + n_3 \hat{\mathbf{e}}_3 \quad (3)$$

where the dot denotes differentiation in time and the prime denotes differentiation in space. Actual distances are given by ax/ϵ where a is the distance between neighboring spins. The scaled time is defined as

$$\tau = 2\sqrt{2}\epsilon s J t. \quad (4)$$

The scaled parameters are related to the parameters in the discrete model by

$$\lambda = \frac{D}{\sqrt{KJ}}, \quad \alpha = \frac{2\sqrt{2}}{\epsilon} s \tilde{\alpha}, \quad \beta = \frac{\tilde{\beta}}{\epsilon^2 J}. \quad (5)$$

For an estimation of the parameters, let us choose $J = 10^{-21}/\hbar \sim 10^{13} \text{ sec}^{-1}$ and $K = 0.01J$, obtaining $\epsilon = 0.1$. If we further choose $J_e \sim 10^{12} \text{ A/m}^2$, $A \sim 10^{-20} \text{ m}^2$ and $b \sim 0.1$, $s \sim 2$, then $\tilde{\beta} \sim 10^{13}$ and $\beta \sim 1$. The scaled parameter β gives the effect of the spin torque due to the polarized current on individual spins of the lattice and it is therefore reasonable that realistic values for this will be a fraction of unity.

Using tetramers, the magnetization takes the form [27]

$$\mathbf{m} = \frac{\epsilon}{2\sqrt{2}} \mathbf{n} \times \dot{\mathbf{n}}. \quad (6)$$

If a one-dimensional antiferromagnet is considered (such as a superlattice structure), then one may only consider dimers and then the magnetization has an additional term $(\epsilon/2)\mathbf{n}'$ [2, 11]. In this paper, we will only consider the magnetization in Eq. (6). The physical spin is $\boldsymbol{\mu} = 4s\mathbf{m}$ at every tetramer site, and the total magnetization \mathbf{M} is found by summing over all tetramers. In the limit $\epsilon \rightarrow 0$, we integrate over space [11] and have the formula

$$\mathbf{M} = \frac{4s}{2\epsilon} \int \mathbf{m} dx = \frac{s}{\sqrt{2}} \int \mathbf{n} \times \dot{\mathbf{n}} dx. \quad (7)$$

The following study starts with the remark that Eq. (3), when no spin current is present, has a static solution which is a standard (180°) domain wall. We will study the dynamics of the domain wall when the spin current is present for various cases of spin polarization.

All numerical results that will be presented in this work have been obtained by simulating the spin lattice using Eq. (2). Our numerical mesh contains 14200 sites and extends from $x = -355$ to $x = 355$. We typically use $s = 1, K/J = 0.0025$ that give $\epsilon = 0.05$. We also set the lattice spacing $a = \epsilon$ for convenience (the value of a does not enter the algorithm for the discrete). If the measured velocity in the simulation is v_s , then the velocity in the continuum theory that will be used for the presentation of results is $v = v_s/(2\sqrt{2}asJ)$ (for the values of a, s, J used in the simulation).

III. PRECESSIONAL DYNAMICS

We consider a spin current with polarization in the direction $\hat{\mathbf{p}} = \hat{\mathbf{e}}_3$. We simulate numerically the discrete Eq. (2) for $\lambda = 0$ (no DM) using as an initial condition a static Néel type domain wall. Eventually, the system reaches a steady state where all spins precess around $\hat{\mathbf{e}}_3$ with constant angular frequency.

For a theoretical study, we will use the spherical parametrization for the Néel vector,

$$n_1 = \sin \Theta \cos \Phi, \quad n_2 = \sin \Theta \sin \Phi, \quad n_3 = \cos \Theta. \quad (8)$$

We set $\lambda = 0$ (no DM) in the following and the equation of motion (3) gives

$$\ddot{\Theta} - \Theta'' + \alpha \dot{\Theta} + \left(1 + \Phi'^2 - \dot{\Phi}^2\right) \sin \Theta \cos \Theta = 0 \quad (9a)$$

$$\sin \Theta \left(\ddot{\Phi} - \Phi'' + \alpha \dot{\Phi} + \beta \right) + 2 \cos \Theta \left(\dot{\Theta} \dot{\Phi} - \Theta' \Phi' \right) = 0. \quad (9b)$$

Anticipating oscillatory dynamics, we assume the simple space and time dependence,

$$\Theta = \Theta(x), \quad \Phi = \Phi(\tau),$$

and substitute in Eqs. (9) to get

$$\Theta'' + \left(\dot{\Phi}^2 - 1 \right) \sin \Theta \cos \Theta = 0, \quad \ddot{\Phi} + \alpha \dot{\Phi} + \beta = 0. \quad (10)$$

The second equation gives

$$\Phi(\tau) = \frac{c}{\alpha} e^{-\alpha\tau} + \omega\tau, \quad \omega = -\frac{\beta}{\alpha}, \quad (11)$$

where c is a constant. The first term decays, giving a stable precession of the Néel vector with frequency ω for large times. Equation (10) for Θ becomes

$$\Theta'' - (1 - \omega^2) \sin \Theta \cos \Theta = 0 \quad (12)$$

and it has the domain wall solution

$$\tan \left(\frac{\Theta}{2} \right) = e^{\pm(x-x_0)/\ell}, \quad \ell = \frac{1}{\sqrt{1-\omega^2}} \quad (13)$$

where x_0 is the position of the wall center. This type of solution was given in [3, 28] for the conservative case, $\alpha = 0, \beta = 0$ and was further discussed in [12]. It is fundamental to distinguish the properties of integer and half-integer spin chains [3]. The precessing domain wall is obtained here as a state which the system spontaneously reaches under spin torque. The solution (13) exists for

$$\omega^2 < 1 \Rightarrow -1 < \frac{\beta}{\alpha} < 1. \quad (14)$$

The Néel vector components are (setting $x_0 = 0$)

$$n_1 + in_2 = \frac{1}{\cosh(x/\ell)} e^{i\omega\tau}, \quad n_3 = \mp \tanh(x/\ell). \quad (15)$$

This form gives a domain wall with the Néel vector precessing around the easy-axis z . It should be noted that the precessional motion of the in-plane components of \mathbf{n} can only be obtained in the presence of a domain wall. While Eq. (12) gives polarized solutions ($\Theta = 0, \pi$) as well as a domain wall solution, it is only in the latter case that the precession around the z axis makes sense. Eq. (12) also has the solutions $\Theta = \pm\pi/2$, but they give polarization perpendicular to the easy axis and are thus unstable.

The conservative model is Lorentz invariant and propagating walls can be obtained by boosting the stationary wall (15) [3]. But, Lorentz invariance is broken in our case due to the damping term and propagating solutions of precessing domain walls do not exist.

We finally note that when a DM term is added in the model, no precessional motion is possible and the standard domain wall solution (for $\omega = 0$) exists. This is because the DM interaction breaks the symmetry of rotations around the z axis.

The magnetization is given by Eq. (7). For the perpendicular component of the total magnetization, we find

$$\mathcal{M}_3 = \frac{4s}{2\epsilon} \int_{-\infty}^{\infty} m_3 dx = \sqrt{2} s \omega \ell = \sqrt{2} s \frac{\omega}{\sqrt{1 - \omega^2}}, \quad (16)$$

a result that is mentioned in [3, 12]. Since m_1, m_2 are odd functions, the in-plane total magnetization is zero. However, it would be useful to find the in-plane magnetization on the left and the right side of the wall. For the right side, it is

$$\mathcal{M}_1 + i\mathcal{M}_2 = \frac{4s}{2\epsilon} \int_0^{\infty} (m_1 + im_2) dx = \mp \frac{s}{\sqrt{2}} \frac{\omega}{\sqrt{1 - \omega^2}} e^{i\omega\tau}.$$

The magnetization diverges to infinity for precession frequencies $\omega \rightarrow 1$ as a result of the domain wall width ℓ in Eq. (13) diverging in the same limit. The significant increase of the magnetization can provide a method for the detection of antiferromagnetic domain walls by either direct measurements of the magnetization or by its possible effect in adjacent magnets.

IV. PROPAGATING WALLS

We now consider a current polarized in the $\hat{\mathbf{p}} = \hat{\mathbf{e}}_2$ direction. We study numerically the behavior of domain walls by solving in time the discrete Eq. (2) using as an initial condition a static Néel type domain wall. Initially, the domain wall is deformed and accelerated. Eventually, the system reaches a steady state propagating with constant velocity. Also, when the simulation starts from a wall which is not perfectly Néel, it still reaches the same steady state. When the simulation starts from a perfectly Bloch wall, this is deformed, but it remains static. Traveling domain walls are obtained with or without the DM term. In the following, we set $D, \lambda = 0$ and study only the case when no DM is present.

Fig. 1 shows the results of simulations for steady-state domain walls for four different values of the parameter β and for damping $\alpha = 1$. The Néel vector at the ends of the wall is tilted with respect to the south and the north pole. This feature is apparent in figures in Ref. [17] but it was not discussed. The wall profile is not symmetric with respect to the center of the wall, a phenomenon that becomes more evident with higher values of β and velocity. For a smaller damping α , the results are similar, but it takes longer to reach the steady state.

For the study of translational motion, we assume the traveling wave ansatz $\mathbf{n} = \mathbf{n}(x - v\tau)$ and the continuum model (3) for the spherical angles gives

$$(1 - v^2)\Theta'' - \left[1 + (1 - v^2)\Phi'^2\right] \sin \Theta \cos \Theta + \alpha v \Theta' = \beta \cos \Phi. \quad (17a)$$

$$(1 - v^2)\Phi'' \sin \Theta + 2(1 - v^2)\Theta' \Phi' \cos \Theta + \alpha v \Phi' \sin \Theta = -\beta \cos \Theta \sin \Phi \quad (17b)$$

where the prime denotes differentiation with respect to the argument $\xi = x - v\tau$. We first look for polarized solutions of Eqs. (17). Setting all derivatives to zero, we have

$$\beta \cos \Phi = -\sin \Theta \cos \Theta, \quad \beta \cos \Theta \sin \Phi = 0.$$

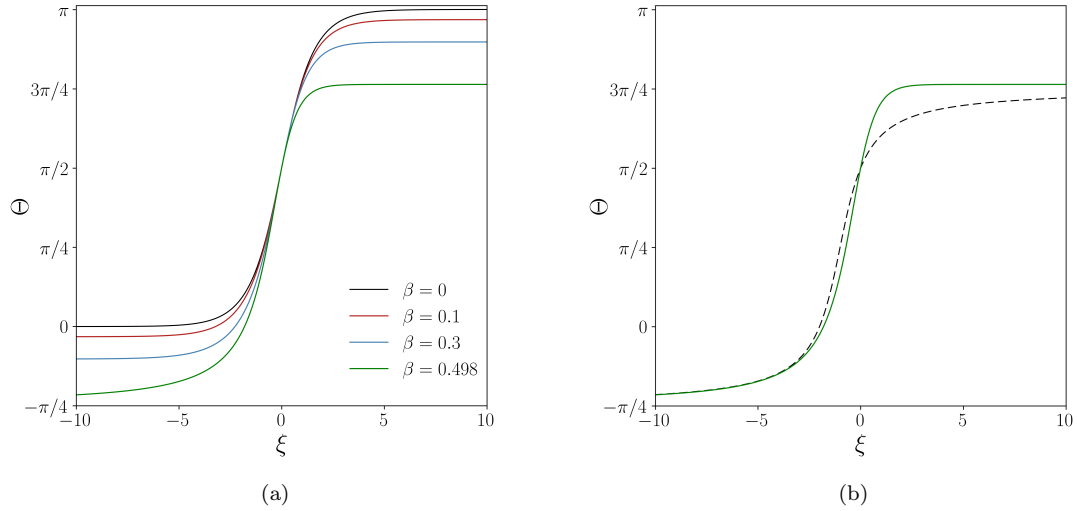


FIG. 1. (a) Traveling domain walls with a constant velocity found numerically for damping parameter value $a = 1$ (the large value of α is used to amplify some features of the wall). The applied spin torques are $\beta = 0.1$, $\beta = 0.3$ and $\beta = 0.498$ (the domain wall for $\beta = 0$ is shown for comparison) and the corresponding velocities are $v \approx 0.156$, $v \approx 0.45$ and $v \approx 0.75$. The Néel vector at the ends of the wall is tilted with respect to the south ($\Theta = \pi$) and the north pole ($\Theta = 0$). The wall profile for $v \neq 0$ is not symmetric with respect to the center of the wall. (b) The numerically obtained domain wall profile (solid line) for $\beta = 0.498$ is compared with the analytical result in Eq. (29) (dashed line). We have power-law decay for $\xi \rightarrow -\infty$ as predicted in (29) but exponential decay for $\xi \rightarrow \infty$.

The second equation shows that nontrivial solutions may be found if we set $\Phi = 0$ or π (i.e., $n_2 = 0$). It is convenient to set $\Phi = 0$ and let $0 \leq \Theta \leq 2\pi$. The first equation gives

$$\sin(2\Theta) = -2\beta \quad \text{for} \quad -\frac{1}{2} < \beta < \frac{1}{2}. \quad (18)$$

Eq. (18) has two pairs of solutions for each value of β . For $\beta = 0$, the first pair of polarized states are $\Theta = 0, \pi$ (pointing to the north and the south poles). For $\beta \neq 0$, these are tilted with respect to the north and the south pole. Let us call this pair $\Theta_P, \pi + \Theta_P$. The domain walls in this system should approach Θ_P and $\pi + \Theta_P$ at the two ends of the spin chain, respectively. The second pair gives polarized states that are on the equator $\Theta = \pi/2, 3\pi/2$ for $\beta = 0$ and are tilted close to the equator for $\beta \neq 0$. The latter represent unstable states, as they are almost orthogonal to the easy axis, and they will not be studied further here.

To find nontrivial solutions for Eq. (17), we note that Eq. (17b) is satisfied for $\Phi = 0$ and Eq. (17a) becomes

$$(1 - v^2) \Theta'' + \alpha v \Theta' = \sin \Theta \cos \Theta + \beta. \quad (19)$$

This is of the form of Newton's equation for a particle in a potential including damping and a constant external force. A perturbed sine-Gordon model that gives Eq. (19) upon using the traveling wave ansatz was employed in Ref. [30] for studying fluxons of magnetic field and their interactions in a Josephson-junction transmission line. A method was presented for studying the dynamics of solitons of the completely integrable sine-Gordon equation under the perturbation.

The magnetization is given by Eq. (7) for $\dot{\mathbf{n}} = -v \mathbf{n}'$. Using the spherical parametrization (8) and setting $\Phi = 0$, we obtain

$$m_1 = 0, \quad m_2 = -\frac{\epsilon v}{2\sqrt{2}} \Theta', \quad m_3 = 0.$$

The total magnetization for a propagating domain wall is

$$\mathcal{M}_2 = -\frac{sv}{\sqrt{2}} \int_{-\infty}^{\infty} \Theta' d\xi = \frac{s\pi}{\sqrt{2}} v. \quad (20)$$

It is in-plane and remains finite for all velocities. A faster wall not only has a higher total moment (20) but, as we shall see in the following, this is also concentrated in a narrower wall width.

Early studies on propagating domain walls in AFM [3, 13, 23] have been based on the Lorentz invariance of the conservative model. We study Eq. (19) where Lorentz invariance is broken due to the presence of damping term, thus going beyond the results of early studies and of more recent work [17, 18].

A. Low currents

A useful formula for the velocity is obtained if we multiply Eq. (19) by Θ' and then integrate to find

$$v \int \Theta'^2 dx = \frac{\beta\pi}{\alpha}, \quad (21)$$

that is valid for all velocities v .

For low currents, $\beta \ll 1$, we assume that the profile of a static domain wall $\Theta(\xi) = \Theta_0(\xi)$ is a good approximation. It is $\Theta_0'' = \sin \Theta_0 \cos \Theta_0 \Rightarrow \Theta_0' = \sin \Theta_0$, which is substituted in Eq. (21) to obtain

$$v \int_{-\infty}^{\infty} \sin \Theta_0 \Theta_0' dx = \frac{\beta\pi}{\alpha} \Rightarrow v \int_0^{\pi} \sin \Theta_0 d\Theta_0 = \frac{\beta\pi}{\alpha} \Rightarrow v = \frac{\pi}{2} \frac{\beta}{\alpha}. \quad (22)$$

More systematic and detailed results can be obtained by applying a perturbation method. We assume the perturbative form

$$\Theta = \Theta_0 + \beta \Theta_1 + O(\beta^2), \quad v = \beta v_1 + O(\beta^2), \quad \beta \ll 1. \quad (23)$$

Substituting in Eq. (19), we obtain, to order $O(1)$, $\Theta_0'' = \sin \Theta_0 \cos \Theta_0$, which corresponds to a standard domain wall. To order $O(\beta)$, we obtain

$$\Theta_1'' - \cos(2\Theta_0)\Theta_1 = 1 - \alpha v_1 \Theta_0'. \quad (24)$$

Following Ref. [31] where a similar equation was studied, we solve Eq. (24) by the method of variation of constants. The homogeneous part of the equation has the explicit basis solutions

$$H_1 = \operatorname{sech}(\xi), \quad H_2 = \sinh(\xi) + \xi \operatorname{sech}(\xi).$$

Using the formula of the variation of constants (with Wronskian $W = 2$), we obtain

$$\Theta_1(\xi) = -\frac{1}{2} H_1(\xi) \int_0^{\xi} (1 - \alpha v_1 \Theta_0') H_2(\tilde{\xi}) d\tilde{\xi} + \frac{1}{2} H_2(\xi) \int_{-\infty}^{\xi} (1 - \alpha v_1 \Theta_0') H_1(\tilde{\xi}) d\tilde{\xi}. \quad (25)$$

This solution satisfies $\Theta_1(0) = 0$, i.e., the domain wall is centered at $\xi = 0$. Satisfying the boundary conditions at $\xi \rightarrow \pm\infty$, imposes the solvability condition

$$\int_{-\infty}^{\infty} [1 - \alpha v_1 \Theta_0'(\tau)] H_1(\tau) d\tau = 0 \Rightarrow \alpha v_1 = \frac{\pi}{2}, \quad (26)$$

where we used $\Theta_0' = -\operatorname{sech}(\xi)$. Thus, for low currents, the velocity is

$$v = \frac{\pi}{2} \frac{\beta}{\alpha}, \quad \text{for} \quad v \ll 1. \quad (27)$$

The result agrees with Eq. (22). The approximation for the velocity (27) was obtained in Ref. [17] by employing a collective coordinate method. The velocity in physical units is $v_{\text{ph}} = 2\sqrt{2}asJv$.

Eq. (25) gives the $O(\beta)$ correction to the static domain wall profile for a propagating wall. It shows that $\Theta_1(\xi)$ is an even function with respect to the value $\frac{\pi}{2}$. Since Θ_0 is odd, we see that the domain wall profile does not have a definite parity with respect to the value $\frac{\pi}{2}$ when $\beta \neq 0$. This is in agreement with the numerical results in Fig. 1.

Figure 2 shows the numerical results for the velocity of the domain wall as a function of the current β for various values of the damping. They are compared with the linear formula (27) found by the perturbation method and are in excellent agreement for small β .

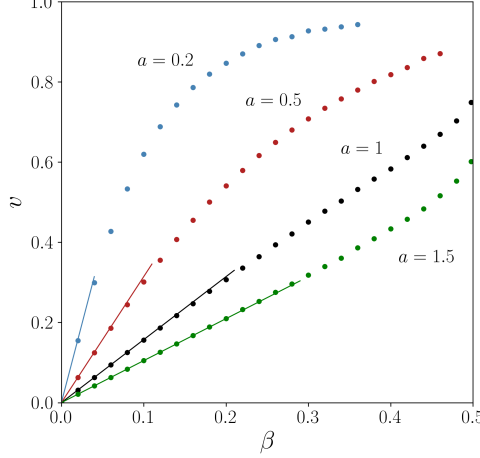


FIG. 2. The velocity v of the propagating domain wall as a function of the parameter β for various values of the damping parameter α . The spin current is polarized in \hat{e}_2 . The solid lines give the theoretical formula for low currents, $v = \frac{\pi}{2} \frac{\beta}{\alpha}$.

B. High currents

Figure 2 shows that for high currents the velocity reaches a maximum. We start the study for high currents by noting that the factor in the first term of Eq. (19) suggests a possible maximum velocity $v = 1$. The equation then reduces to

$$\alpha\Theta' = \frac{1}{2} \sin(2\Theta) + \beta. \quad (28)$$

For any $0 \leq \beta < \frac{1}{2}$, the right side of the equation gives that Θ' is zero not only at Θ_P and $\pi + \Theta_P$ but also for some intermediate value $\Theta_P < \Theta < \pi + \Theta_P$. This is a fixed point of Eq. (28) and therefore there is no solution connecting Θ_P with $\pi + \Theta_P$. As a conclusion, there is no domain wall for $0 \leq \beta < \frac{1}{2}$ which can reach the velocity value $v = 1$. In Refs. [32, 33], Eq. (19) was studied numerically as a model for magnetic fluxons [30]. It is suggested that $v = 1$ is obtained for $\beta < 1/2$, but these numerical results in the high velocity regime do not agree with our previous analytical arguments.

The numerical results shown in Fig. 2 are in agreement with the previous observation. For small values of α , the current parameter β can be varied up to a maximum value that is less than $1/2$ and the velocity gets close to $v = 1$ but it does not reach this value. Above this maximum value for β , our simulation does not converge to a propagating domain wall. For higher values of α , the limiting value for β increases and it can be very close to $\beta = 1/2$. In this case, the velocity remains clearly below unity. We see that the limiting velocity increases as the damping parameter α decreases.

For $\beta = \frac{1}{2}$ and $v = 1$, Eq. (19) gives

$$\alpha\Theta' = \frac{1}{2} [1 + \sin(2\Theta)]$$

and has the solution

$$\tan\left(\Theta - \frac{\pi}{4}\right) = \frac{\xi - \xi_0}{\alpha} \quad \text{or} \quad \tan\Theta = \frac{\alpha + (\xi - \xi_0)}{\alpha - (\xi - \xi_0)}, \quad (29)$$

where ξ_0 is an arbitrary constant. Choosing $\xi_0 = -\alpha$, sets $\Theta(\xi = 0) = \pi/2$. This form represents a domain wall with $\Theta_P = -\pi/4$, $\pi + \Theta_P = 3\pi/4$ at the two ends of the system $x = \pm\infty$, and a width proportional to the damping parameter α . The form (29) has some unusual features. The first is that the wall profile is strongly asymmetric around the center of the wall. The second is that it approaches the limiting values following a power law (since $\arctan x = \pm\frac{\pi}{2} \mp \frac{1}{x} + \dots$ at $|x| \rightarrow \infty$), in contrast to the typical exponential decay for the standard domain wall. The power-law decay is due to the specific limiting value Θ_P . Any $\beta \neq 1/2$ would give different Θ_P and an exponential decay of the wall profile at large distances.

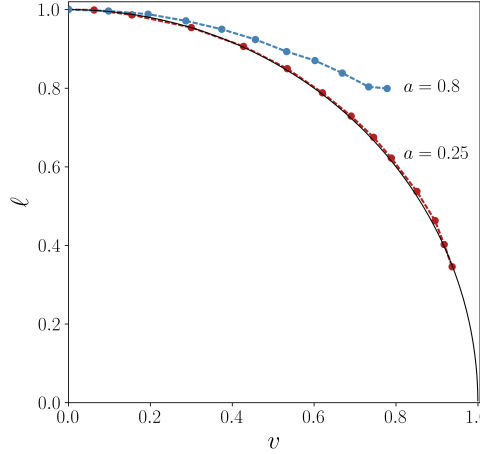


FIG. 3. Propagating domain wall width, defined as $\ell = 1/\Theta'$ at the point with $\Theta = \pi/2$, as a function of the velocity v for damping parameter values $\alpha = 0.25$ (red) and $\alpha = 0.8$ (blue). The maximum velocity is below the value $v = 1$ for both values of α . The solid line (black) gives the domain wall width in the Lorentz invariant case, $\ell = \sqrt{1 - v^2}$.

Our numerical results show that although the domain wall profile (29) is not achieved, it nonetheless describes some main features of the profiles, such as that shown in Fig. 1b, as we will now explain. When β is close to the value 1/2, the velocity is $v < 1$ and Eq. (19) gives a solution $\Theta \sim e^{-\alpha v/(1-v^2)\xi}$ at the ends of the wall. The exponential decay is valid for $\xi \rightarrow \infty$, but it is not an acceptable solution at the other end of the wall. Instead, at $\xi \rightarrow -\infty$, the solution presents a power-law decay as in the form (29). Fig. 1b shows a domain wall profile for $\beta = 0.498$ exhibiting asymmetry and different decay behaviors at $x \rightarrow \pm\infty$.

Combining the analytical with numerical results, we can now give a full description of the domain wall for low and high velocities. For small values of the damping α , the velocity initially increases rapidly with β following the perturbative result (27). It reaches a maximum value $v < 1$ for a current $\beta < 1/2$. The profile of the domain wall at high velocities is similar to the form (29) in its central part, but it decays exponentially at large distances. For large α , the initial linear increase of the velocity with β is slower. As β approaches the value 1/2, the velocity takes its maximum value which is smaller than unity.

We define $\ell = 1/\Theta'$ at the point where $\Theta = \pi/2$, which can be considered as a measure of the width of the domain wall. Fig. 3 shows that ℓ decreases with v , but remains greater than the damping parameter α , which is the width of the wall in Eq. (29). For small α , it seems to follow the form $\ell = \sqrt{1 - v^2}$ of the Lorentz invariant equation (although the maximum possible velocity is smaller than unity). This is a surprising result for two reasons. First, for larger β , the term that breaks the Lorentz invariance is not small. Second, the first order correction of the wall profile in Eq. (25) is unrelated to the factor $1 - v^2$ in Eq. (19). For larger α , we have large deviations from the Lorentz invariant formula. It should be emphasized that ℓ may not be an accurate definition of the domain wall width, especially for larger β where the wall profile is strongly asymmetric.

V. DOMAIN WALL OSCILLATIONS

In Sec. V, we saw that currents polarized along \hat{e}_3 cause precession of the domain wall while, in Sec. IV, we saw that currents polarized along \hat{e}_2 cause domain wall propagation. We now choose a current with $\beta\hat{p} = \beta_2\hat{e}_2 + \beta_3\hat{e}_3$. We consider an initially static Néel-type domain wall and solve numerically the spin equations (2). We typically use $\beta_2 = \beta_3$. The simulations show that, after a transient period, a domain wall undergoes oscillatory motion.

Figure 4 shows three snapshots of the simulation after the oscillatory motion has been established. Only the central part of the numerical mesh is shown in the snapshots. The wall is seen to move periodically between two end positions, $-x_{\min} < x < x_{\max}$. The profile of the wall is shown approximately at the left end position, at a central position, and at the right end position of the motion. While the wall position oscillates, \mathbf{n} is precessing around the easy axis, as seen by the change of its in-plane components.

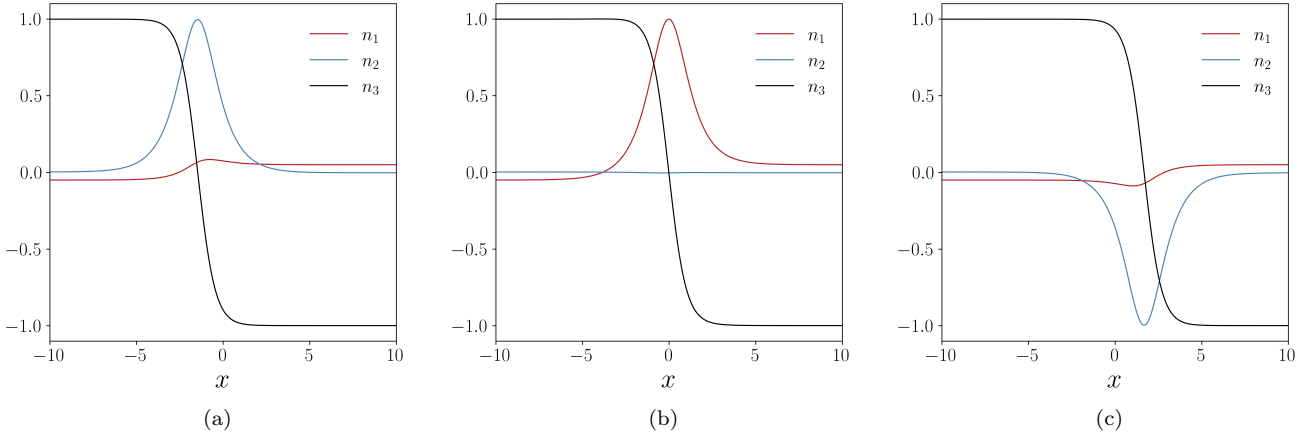


FIG. 4. Under spin current with $\beta\hat{\mathbf{p}} = \beta_2\hat{\mathbf{e}}_2 + \beta_3\hat{\mathbf{e}}_3$, the domain wall undergoes oscillatory motion, moving periodically between two end positions, $-x_{\min} < x < x_{\max}$. The domain wall is shown at approximately (a) the left end position $x = x_{\min}$, (b) at a central position, and (c) at the right end position $x = x_{\max}$ of the motion. The parameters are $\beta_2 = \beta_3 = 0.05$ and $\alpha = 1$. The in-plane components indicate that the Néel vector is precessing during the motion.

For an understanding of the oscillating motion of the domain wall, we write the equations for Θ, Φ ,

$$\ddot{\Theta} - \Theta'' + \alpha\dot{\Theta} + (1 + \Phi'^2 - \dot{\Phi}^2) \sin\Theta \cos\Theta = -\beta_2 \cos\Phi \quad (30a)$$

$$\sin\Theta (\ddot{\Phi} - \Phi'' + \alpha\dot{\Phi} + \beta_3) + 2\cos\Theta (\dot{\Theta}\dot{\Phi} - \Theta'\Phi') = \beta_2 \cos\Theta \sin\Phi. \quad (30b)$$

We expect that β_3 will induce precession of the Néel vector with angular frequency $\omega = -\beta_3/\alpha$ as obtained in Sec. V, Eq. (11). Propagation of the domain wall will be induced by β_2 . Assuming $\Phi = \omega\tau$ and $\Theta = \Theta(x - v\tau)$, Eq. (30a) becomes

$$(1 - v^2)\Theta'' + \alpha v\Theta' - (1 - \omega^2) \sin\Theta \cos\Theta = -\beta_2 \cos(\omega\tau). \quad (31)$$

This is similar in form to Eq. (19) which was studied in Sec. IV. We may tentatively use the result in Eq. (27), which now takes the form

$$v = \frac{\pi}{2} \frac{\beta_2}{\alpha} \cos\left(\frac{\beta_3}{\alpha}\tau\right). \quad (32)$$

This gives periodic oscillations of the domain wall. Figure 5a shows the position and Fig. 5b the velocity of the domain wall for the simulation in Fig. 4. Figure 5b shows also a comparison between the velocity of the domain wall and the theoretical result (32). The agreement is excellent regarding both the amplitude and the frequency of oscillations.

The result (32) is expected to be valid for low velocities, $|v| \ll 1$, since it is based on the perturbative method of Sec. IV. Also, we have ignored Eq. (30b), which should be a valid approximation for $|\omega| \ll 1$. In conclusion, the result (32) is expected to be valid for $\beta_2, \beta_3 \ll 1$, which also imply $|v|, |\omega| \ll 1$. Nevertheless, the accuracy of the result (32) for the simulation in Fig. 5 is surprising given the approximations involved in its derivation.

VI. CONCLUDING REMARKS

We studied the dynamics of antiferromagnetic domain walls under spin-orbit torques. All simulations have been performed using the spin equations (2), while the theoretical analysis is based on the continuum model (3). This model is built upon an extension of the σ -model and in addition it contains damping and source terms.

We find that the system spontaneously converges to a stationary state and the result depends on the spin polarization of the injected current. Precessional dynamics, analogous to that discussed in early papers for the conservative model, is obtained as a stable steady state for perpendicular spin current polarization. Propagation of a domain wall with a constant velocity is obtained for in-plane spin current polarization perpendicular to the in-plane component of the

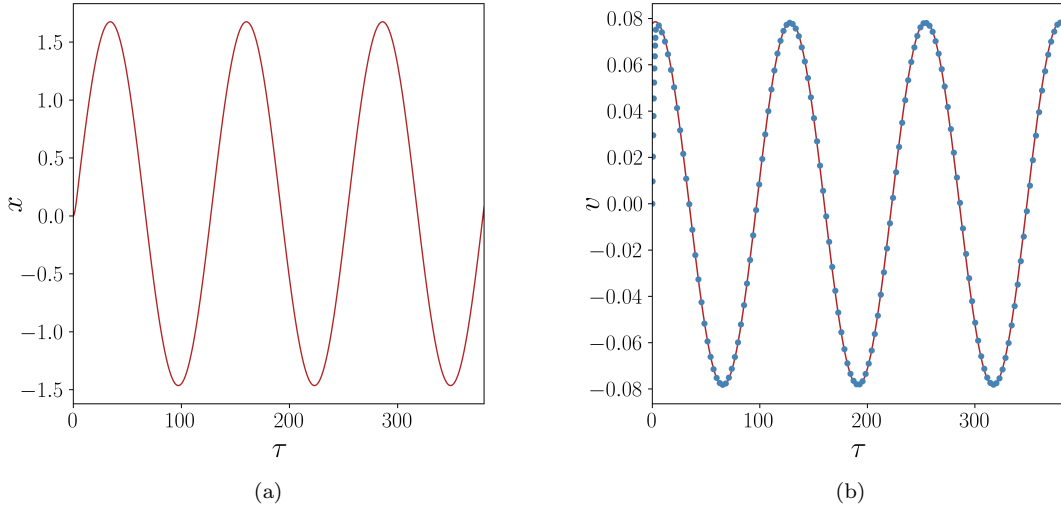


FIG. 5. (a) The position x for an oscillating domain wall as a function of time given by a simulation for parameter values $\beta_2 = \beta_3 = 0.05$ and $a = 1$. (b) The velocity v in the simulation is shown by blue points. This is compared with the result (32) shown by a red solid line. It is seen that the system quickly achieves the oscillating steady state.

wall. The details of the dynamics are not drawn from a Lorentz transformation of the static wall, unlike in the conservative case. Instead, different methods are applied for finding solutions of the model and studying their main features. Periodic motion of the wall between two positions is obtained for a current polarization with both an in-plane and a perpendicular component. The present study is based on a model that describes the antiferromagnet under spin current and obtains results beyond those inferred by the idealized σ -model.

We discuss the magnetic moment carried by dynamical antiferromagnetic domain walls. This depends on the wall dynamics and may also depend on the wall profile. For example, propagating walls have a magnetization proportional to the velocity and their width decreases with increasing velocity. As a result, faster walls have a higher local moment density and a higher total moment. However, this is bounded by the moment of a single spin. By contrast, precessing walls can have an arbitrarily large total moment for high precession frequencies. The net moment in antiferromagnets could give a handle for the observation and manipulation of AFM textures. Given the recent progress in methods to observe AFM order, we hope that our results will motivate detailed observations of domain wall dynamics and will help develop processes for transmission of information or logic gate implementations.

ACKNOWLEDGMENTS

G. Theodorou gratefully acknowledges support from the ERC starting grant 101078061 SINGinGR, under the European Union's Horizon Europe program for research and innovation. This work has greatly benefited from networking activities of the COST Action Polytopo, CA23134, supported by COST (European Cooperation for Science and Technology).

[1] A. M. Kosevich, B. A. Ivanov, and A. S. Kovalev, *Physics Reports* **194**, 117 (1990).
[2] H.-J. Mikeska and M. Steiner, *Advances in Physics* **40**, 191 (1991).
[3] F. D. M. Haldane, *Phys. Rev. Lett.* **50**, 1153 (1983).
[4] S.-W. Cheong, M. Fiebig, W. Wu, L. Chapon, and V. Kiryukhin, *npj Quantum Materials* **5**, 3 (2020).
[5] N. Hedrich, K. Wagner, O. V. Pylypovskiy, B. J. Shields, T. Kosub, D. D. Sheka, D. Makarov, and P. Maletinsky, *Nature Physics* **17**, 574 (2021).
[6] V. Grigorev, M. Filianina, Y. Lytvynenko, S. Sobolev, A. R. Pokharel, A. P. Lanz, A. Sapozhnik, A. Kleibert, S. Bodnar, P. Grigorev, Y. Skourski, M. Kläui, H.-J. Elmers, M. Jourdan, and J. Demsar, *ACS Nano* **16**, 20589 (2022).

- [7] T. Sato, N. Abe, Y. Tokunaga, and T.-h. Arima, *Phys. Rev. B* **105**, 094417 (2022).
- [8] H. Meer, S. Wust, C. Schmitt, P. Herrgen, F. Fuhrmann, S. Hirtle, B. Bednarz, A. Rajan, R. Ramos, M. A. Niño, M. Foerster, F. Kronast, A. Kleibert, B. Rethfeld, E. Saitoh, B. Stadtmüller, M. Aeschlimann, and M. Kläui, *Advanced Functional Materials* **33**, 2213536 (2023).
- [9] P. Wadley, S. Reimers, M. J. Grzybowski, C. Andrews, M. Wang, J. S. Chauhan, B. L. Gallagher, R. P. Campion, K. W. Edmonds, S. S. Dhesi, F. Maccherozzi, V. Novak, J. Wunderlich, and T. Jungwirth, *Nature Nanotechnology* **13**, 362 (2018).
- [10] L. Baldrati, O. Gomonay, A. Ross, M. Filianina, R. Lebrun, R. Ramos, C. Leveille, F. Fuhrmann, T. R. Forrest, F. Maccherozzi, S. Valencia, F. Kronast, E. Saitoh, J. Sinova, and M. Kläui, *Phys. Rev. Lett.* **123**, 177201 (2019).
- [11] N. Papanicolaou, *Phys. Rev. B* **51**, 15062 (1995).
- [12] B. A. Ivanov and A. K. Kolezhuk, *Phys. Rev. Lett.* **74**, 1859 (1995).
- [13] E. G. Galkina and B. A. Ivanov, *Low Temp. Phys.* **44**, 618 (2018).
- [14] S. Komineas and N. Papanicolaou, *SciPost Phys.* **8**, 086 (2020).
- [15] T. Jungwirth, X. Marti, P. Wadley, and J. Wunderlich, *Nature Nanotechnology* **11**, 231 (2016), arXiv:1509.05296v1.
- [16] A. Dal Din, O. J. Amin, P. Wadley, and K. W. Edmonds, *npj Spintronics* **2**, 25 (2024).
- [17] T. Shiino, S.-H. Oh, P. M. Haney, S.-W. Lee, G. Go, B.-G. Park, and K.-J. Lee, *Phys. Rev. Lett.* **117**, 087203 (2016).
- [18] O. Gomonay, T. Jungwirth, and J. Sinova, *Phys. Rev. Lett.* **117**, 017202 (2016).
- [19] L. Sánchez-Tejerina, V. Puliafito, P. Khalili Amiri, M. Carpentieri, and G. Finocchio, *Phys. Rev. B* **101**, 014433 (2020).
- [20] A. C. Swaving and R. A. Duine, *Phys. Rev. B* **83**, 054428 (2011).
- [21] K. M. D. Hals, Y. Tserkovnyak, and A. Brataas, *Phys. Rev. Lett.* **106**, 107206 (2011).
- [22] E. G. Tveten, A. Qaiumzadeh, and A. Brataas, *Phys. Rev. Lett.* **112**, 147204 (2014).
- [23] I. V. Bary'akhtar and B. A. Ivanov, *Sov. Phys. JETP* **58**, 190 (1983).
- [24] N. Papanicolaou, *J. Phys.: Condensed Matter* **10**, L131 (1998).
- [25] M. Bode, E. Y. Vedmedenko, K. von Bergmann, A. Kubetzka, P. Ferriani, S. Heinze, and R. Wiesendanger, *Nature Materials* **5**, 477 (2006).
- [26] H. T. Hirose, J.-i. Yamaura, and Z. Hiroi, *Scientific Reports* **7**, 42440 (2017).
- [27] S. Komineas and N. Papanicolaou, *Nonlinearity* **11**, 265 (1998).
- [28] I. V. Bary'akhtar and B. A. Ivanov, *Sov. J. Low Temp. Phys.* **5**, 361 (1979).
- [29] H. V. Gomonay and V. M. Loktev, *Phys. Rev. B* **81**, 144427 (2010).
- [30] D. W. McLaughlin and A. C. Scott, *Phys. Rev. A* **18**, 1652 (1978).
- [31] S. Komineas, C. Melcher, and S. Venakides, *Physica D* **418**, 132842 (2021).
- [32] K. Nakajima, Y. Onodera, T. Nakamura, and R. Sato, *J. Appl. Phys.* **45**, 4095 (1974).
- [33] K. Nakajima, T. Yamashita, and Y. Onodera, *J. Appl. Phys.* **45**, 3141 (1974).